Nanoscale Research Letters

NANO EXPRESS Open Access

Interface-Induced WSe_2 In-plane Homojunction for High-Performance Photodetection

Jiawei Chi[1,2], Nan Guo[1*], Yue Sun[1], Guohua Li[2] and Lin Xiao[1*]

Abstract

2D transition metal dichalcogenides (TMDCs) have been extensively attractive for nano-electronics and nano-optoelectronics due to their unique properties. Especially, WSe_2, having bipolar carrier transport ability and sizable bandgap, is a promising candidate for future photodetectors. Here, we report an in-plane WSe_2 homojunction formed by the interface gate of the substrate. In this architecture, an insulated h-BN flake was used to make only part of WSe_2 flake contact substrate directly. Finally, the structures of WSe_2/substrate and WSe_2/h-BN/substrate construct an in-plane homojunction. Interestingly, the device can operate in both photovoltaic and photoconductive modes at different biases. As a result, a responsivity of 1.07 A W^{-1} with a superior detectivity of over 10^{12} jones and a fast response time of 106 μs are obtained simultaneously. Compared with previously reported methods adopted by chemical doping or electrostatic gating with extra bias voltages, our design provides a more facile and efficient way for the development of high-performance WSe_2-based photodetectors.

Keywords: Transition metal dichalcogenides, In-plane homojunction, Photodetection, Interface gate

Introduction

In recent decade, 2D transition metal dichalcogenides (TMDCs) have drawn great attention owing to their particular properties. High in-plane mobility, tunable bandgap, mechanical flexibility, strong light-matter interaction, and easy processing make them very competitive for future nano-optoelectronics devices [1–20]. Especially, tungsten diselenide (WSe_2), a bipolar semiconductor with facile carrier-type manipulation, allows remarkably potential applications in the junction-based photodetectors [21–28]. So far, the main strategies of constructing junction solely in WSe_2 include chemical doping and electrostatic gating. For example, recently, an intramolecular WSe_2 p-n junction was reported [26]. The n region and p region within WSe_2 were formed by polyethyleneimine chemical doping and back gate control, respectively. The p-n junction presented a responsivity of 80 mA W^{-1} and 200 μs response time. Sun et al. doped WSe_2 by using cetyltrimethyl ammonium bromide to form intramolecular p-n junction, in which the responsivity and the response time are 30 A W^{-1} and ~ 7 ms, respectively [27]. Baugher et al. demonstrate a lateral WSe_2 p-n junction achieved by electrostatic gating through applying two gate biases with opposite polarity. The responsivity of 210 mA W^{-1} has been obtained [28]. However, due to the inevitable chemical impurities and the necessary multiple bias settings, these methods make the fabrication and application of junction-based devices complex and difficult. Assembling various 2D materials to build vertical van der Waals heterostructures like WSe_2/MoS_2 junction [29] has become popular for the development of novel photodetectors. But, in this configuration, the process of carrier transport between different layered materials suffers from the interface defects, which restricts the device response speed. For the Schottky junction formed between metals and 2D materials, the Schottky barrier height is usually

* Correspondence: guonan@qxslab.cn; xiaolin@qxslab.cn
[1]Qian Xuesen Laboratory of Space Technology, China Academy of Space Technology, Beijing 100094, China
Full list of author information is available at the end of the article

determined by Fermi-level pinning, which is uncontrollable and has a great impact on the responsivity of the devices. Additionally, the reported works cannot seem to possess both high responsivity and fast response speed.

Here, we demonstrate a facile and more efficient way to realize an in-plane WSe_2 homojunction. In the architecture, part of WSe_2 channel is on the Si/SiO_2 substrate and the other part is on the h-BN flake. This scheme is common in floating/semi-floating gate memories, in which the h-BN is adopted as gate dielectric layer [30, 31]. The charges stored on one side of h-BN layer can regulate the conductivity of the material on the other side. In our work, however, the h-BN flake as a perfect isolator is used to eliminate the interface gating effect on the WSe_2 channel. The polarity of WSe_2, which part is only on the Si/SiO_2 substrate, can be modulated by interface gate. As a result, the devices operate in photovoltaic (PV) mode well at zero bias. Meanwhile, it exhibits photoconductive (PC) characteristics at high bias. A responsivity of 1.07 A W^{-1} with a superior detectivity of over 10^{12} jones and a fast response time of 106 μs are obtained simultaneously without the intricate device design and the risk of introducing additional chemical impurities.

Results and Discussion

Figure 1a shows a schematic of the in-plane WSe_2 homojunction. It can be seen that part of WSe_2 flake is placed on h-BN flake (WSe_2-h) and the other part contacts the Si/SiO_2 substrate directly (WSe_2-S). The function of h-BN is to isolate the interface gate (IG) of the Si/SiO_2 substrate on the WSe_2-h. So, the formation of homojunction between WSe_2-h and WSe_2-S mainly relies on the IG modulating the polarity of WSe_2-S. The

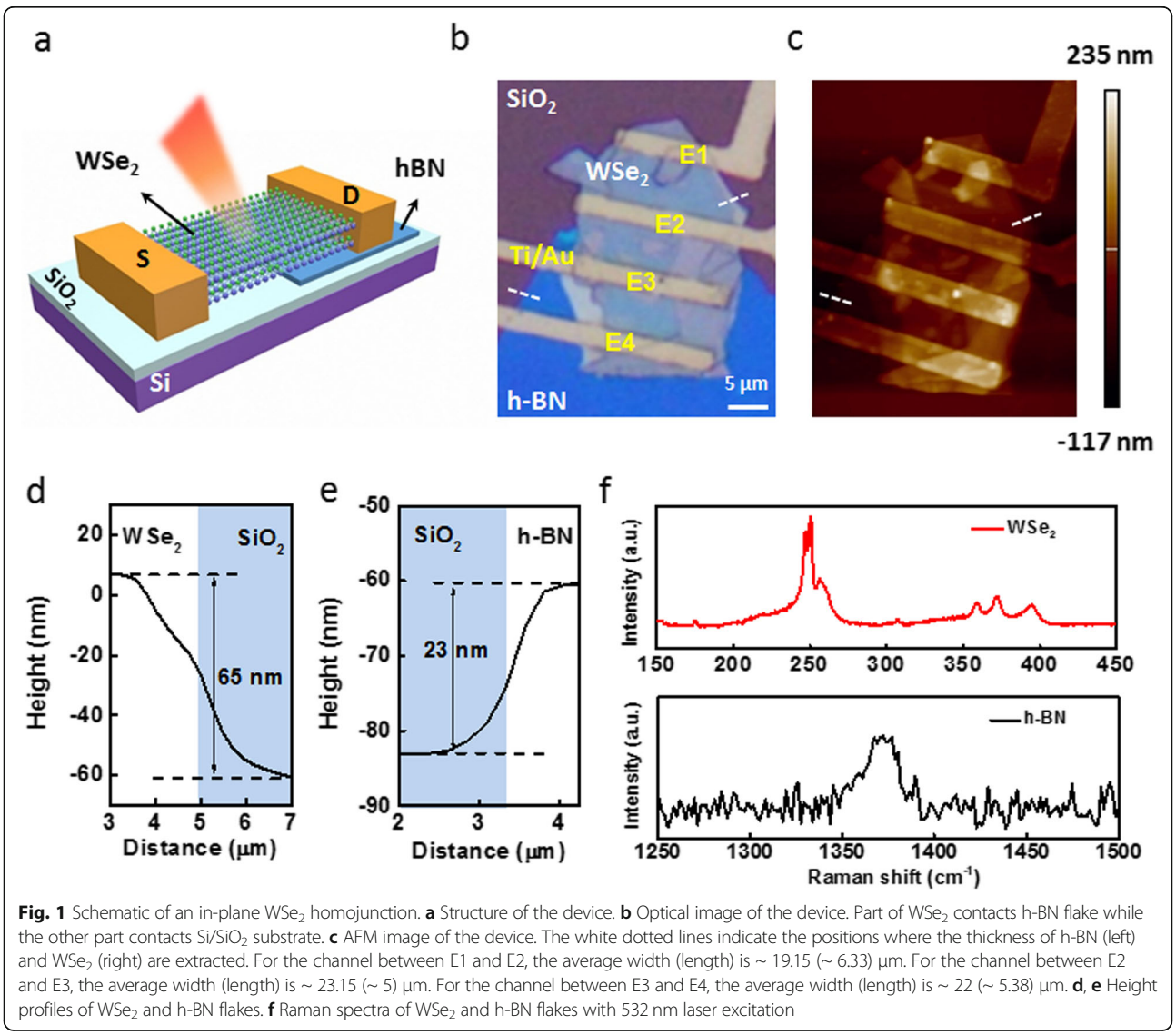

Fig. 1 Schematic of an in-plane WSe_2 homojunction. **a** Structure of the device. **b** Optical image of the device. Part of WSe_2 contacts h-BN flake while the other part contacts Si/SiO_2 substrate. **c** AFM image of the device. The white dotted lines indicate the positions where the thickness of h-BN (left) and WSe_2 (right) are extracted. For the channel between E1 and E2, the average width (length) is ~ 19.15 (~ 6.33) μm. For the channel between E2 and E3, the average width (length) is ~ 23.15 (~ 5) μm. For the channel between E3 and E4, the average width (length) is ~ 22 (~ 5.38) μm. **d**, **e** Height profiles of WSe_2 and h-BN flakes. **f** Raman spectra of WSe_2 and h-BN flakes with 532 nm laser excitation

IG is produced by the trapped charges at the SiO_2 surface. This will be discussed below in detail. Figure 1b presents the optical picture of the device. Four electrodes (E1-E4, Ti/Au) were prepared by electron-beam lithography, metallization, and the lift-off process. The thickness of materials is characterized by atomic force microscope (AFM) (see Fig. 1c). The height of WSe_2 (h-BN) flake in direct contact with the Si/SiO_2 substrate (white dotted lines) was measured as 65 (23) nm (see Fig. 1d, e). It can be seen that there is a slope instead of sharp step in the height profile between the WSe_2 (h-BN) and the Si/SiO_2 substrate. This may be due to the residual photoresist at the edge of the material. Figure 1f shows the Raman spectra of WSe_2 and h-BN flakes. For the WSe_2, the first order E_{2g} and A_{1g} Raman modes are clearly distinguished ~ 250 cm^{-1}, suggesting that the WSe_2 has a multilayer morphology [32, 33]. For the h-BN, the Raman peak of E_{2g} mode at ~ 1370 cm^{-1} is observed. Due to the large bandgap of h-BN, the Raman signal is weak compared with that in WSe_2 [34].

To explore the effect of substrate on WSe_2, transfer characteristics of WSe_2-S and WSe_2-h were studied separately. As shown in Fig. 2a, both transfer curves exhibit bipolar behavior and an obvious hysteresis can be observed in the curve of WSe_2-S (black) compared with that of WSe_2-h (red). The current of WSe_2-h is higher than that of WSe_2-S. The steep slope in the curve of WSe_2-h indicates a relatively large transconductance, which is proportional to carrier mobility. For WSe_2-S, the hysteresis is attributed to the charge trapping at the SiO_2 surface [35–38]. When V_g was swept from − 30 to 0 V, the negative V_g makes the WSe_2 populated with holes and drives some holes into the SiO_2 (see Fig. 2b). The trapped holes in SiO_2 generate a positive local gate, i.e., IG, to modulate the WSe_2 conductance in return (weak depletion effect). Therefore, the charge neutrality point of V_g appears around − 5 V. Similarly, when V_g was swept from 30 to 0 V, the positive V_g makes the WSe_2 populated with electrons and also drives some electrons into the SiO_2 (see Fig. 2c). The trapped electrons in SiO_2 generate a negative IG to modulate the WSe_2 conductance in return (the same weak depletion effect). So, the charge neutrality point of V_g appears around 5 V. For WSe_2-h, the h-BN flake inhibits the carrier transfer between WSe_2 and SiO_2 under V_g modulation. This is the reason for the non-obvious hysteresis in the WSe_2-h curve. Therefore, an in-plane homojunction can be formed simply by taking advantage of the IG.

Figure 3a shows the I_d-V_d curves of the device under dark and light conditions at V_g = 0 V. The source-drain voltage is applied on electrodes E2 and E3 (see the inset). It can be seen that the short-circuit currents (at V_d = 0 V) increase with the incident power, indicating a PV effect. Interestingly, the curves also present PC characteristics at V_d = ± 1 V. For the former, the photocurrents are attributed to the homojunction. As shown in Fig. 3b, although V_d and V_g were set at 0 V, a few already trapped holes in SiO_2 form a small positive IG to modulate the WSe_2-S. So, the n^--type WSe_2-S and intrinsic WSe_2-h (without the effect of IG due to the isolation by h-BN flake) constitute an in-plane homojunction. Under illumination, the photoexcited electron-hole pairs will be separated by built-in field of the homojunction. Although I_d-V_d curves present PV characteristic well at zero bias, the homojunction did not show a rectifying behavior maybe due to the relatively weak built-in field compared with the externally applied V_d. For the latter, the whole WSe_2 flake as a photoconductor responds the light signal at high bias. The photoexcited carriers will be driven to the electrodes by V_d. Therefore, the photoresponse in Fig. 3a is the result of synergistic effect of PV and PC modes. The responsivities as a function of the light power for different V_d are summarized in Fig. 3c, given by $R = I_{ph}/PA$, where I_{ph} is the photocurrent, P is the power intensity, and A is the effective photosensitive area of the detector [39, 40]. During the calculation, the effective photosensitive area, i.e., the WSe_2 part between E2 and E3, is 115.75 μm^2. The responsivities of 1.07 A W^{-1} and 2.96 A W^{-1} are obtained for V_d of 0 V

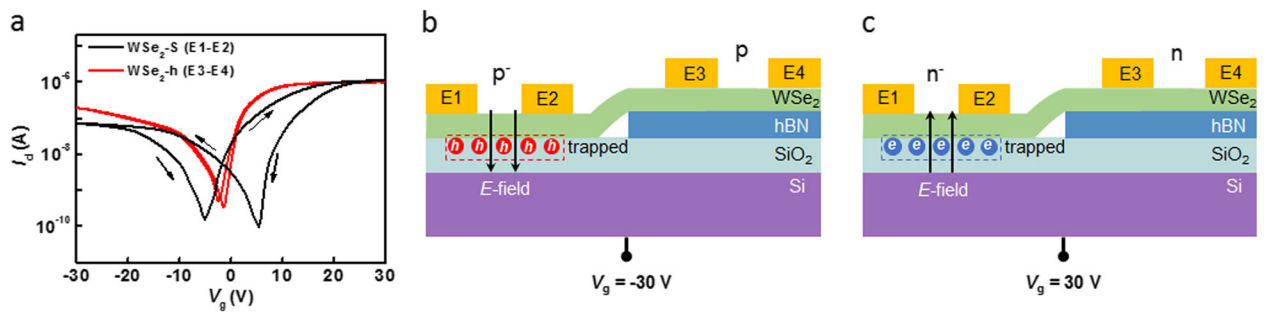

Fig. 2 Transfer characteristics. **a** I_d-V_g curves of WSe_2-S (black line) and WSe_2-h (red line). The sweep direction of V_g is indicated by the arrows. **b**, **c** Physical explanation for the hysteresis phenomenon. The arrows indicate the direction of electric field induced by V_g. The red and blue spheres represent holes and electrons, respectively

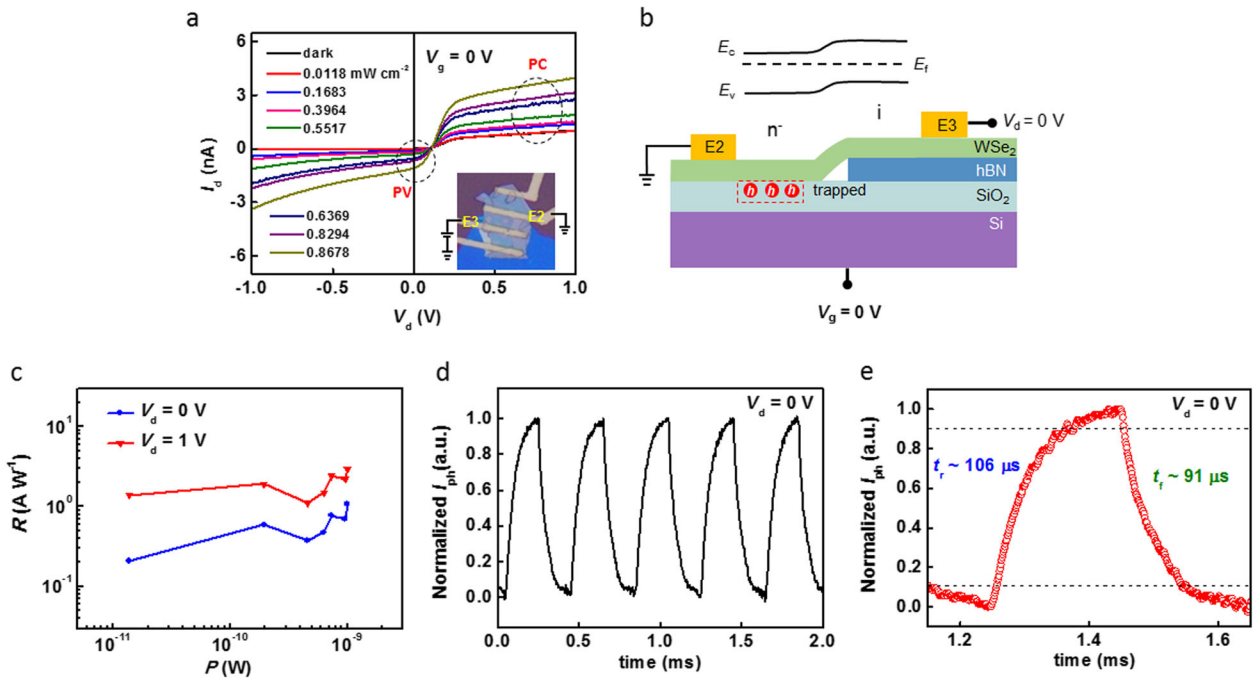

Fig. 3 Photoresponse performance of the homojunction acquired between E2 and E3. **a** Drain current as a function of source-drain voltage applied on electrodes E2 and E3 (see the inset) with variable light power intensity (637 nm). **b** Formation mechanism of the homojunction at V_g = 0 V and V_d = 0 V. **c** Responsivity as a function of light power. **d**, **e** Temporal response of the device acquired at V_d = 0 V for 637 nm illumination. An oscilloscope was used to monitor the time dependence of the current

and 1 V, respectively. The specific detectivity (D^*) as an important parameter determines the capability of a photodetector to response a weak light signal. Assuming that the shot noise from the dark current is the major contribution, D^* can be defined as $D^* = RA^{1/2}/(2eI_{dark})^{1/2}$, where R is the responsivity, A is the effective photosensitive area, e is the electron charge, and I_{dark} is the dark current [41, 42]. Benefitting from the extremely low I_{dark}, D^* of 3.3 × 10^{12} jones (1 jones = 1 cm $Hz^{1/2}$ W^{-1}) and 1.78 × 10^{11} jones are achieved for V_d of 0 V and 1 V, respectively. Moreover, response time as a key figure of merit has been studied. As shown in Fig. 3d, a high and a low current state acquired at V_d = 0 V have been obtained with the light modulation. The transient photoresponse exhibits highly stable and reproducible characteristics. Figure 3e gives a single modulation cycle of temporal response. The rising time (t_r), defined as the time necessary for the current to increase from 10% I_{peak} to 90% I_{peak}, was found to be ~ 106 μs, and the falling time (t_f), defined analogously, was found to be ~91 μs. Figure S1 shows temporal response of the device acquired at V_d = 1 V. t_r and t_f were found to be ~105 μs and ~ 101 μs, respectively. Table 1 summarizes the reported WSe_2 homojunction formed by different methods. Obviously, the device in our work has high D^*, comparable R, and relatively fast response speed. Moreover, Figure S2 presents the photoresponse characteristics of the other three devices. Distinct PV and PC currents can be observed at zero and high bias, respectively. The detectivity of all the WSe_2 homojunctions is higher than 10^{12} jones, and the response time is a little more than 100 μs, proving that our devices can repeat the high-performance photodetection very well.

Figure 4a and b present the I_d-V_d characteristics of WSe_2-h and WSe_2-S separately. The curves of both

Table 1 Optoelectronic characteristics of WSe_2 homojunction formed by different methods

WSe_2 homojunction formed by	Wavelength (nm)	Responsivity (A W^{-1})	Detectivity (jones)	Time	References
h-BN/two gates	532	7 × 10^{-4}	-	10 ms	24
SiN/two gates	500–900	0.016	-	-	25
Polyethylene imine chemical doping	520	0.08	10^{11}	200 μs	26
Cetyltrimethyl ammonium bromide chemical doping	450	30	10^{11}	7.8 ms	27
HfO_2/two gates	532	0.21	-	-	28
h-BN/interface gate	637	1.07	10^{12}	106 μs	This work

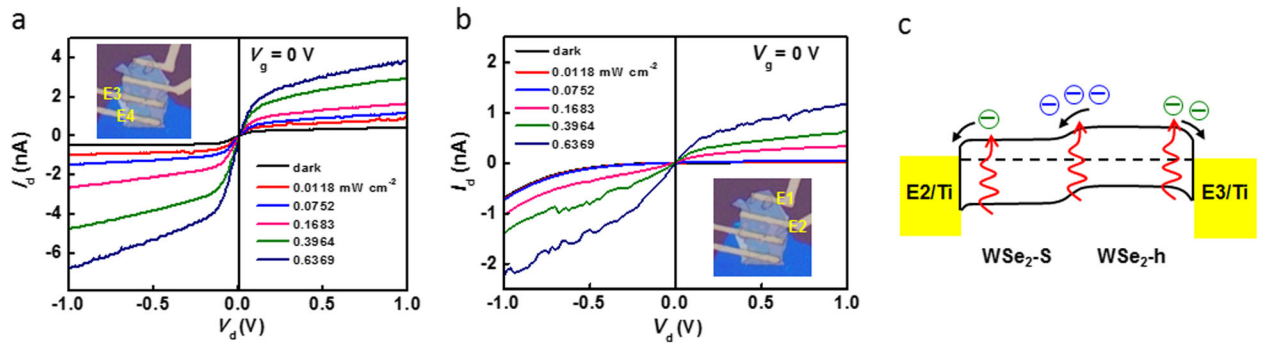

Fig. 4 Effect of Schottky junction on photoresponse. **a** I_d-V_d curves of WSe_2-h with source-drain voltage applied on electrodes E3 and E4 (see the inset) under light illumination (637 nm). **b** I_d-V_d curves of WSe_2-S with source-drain voltage applied on electrodes E1 and E2 (see the inset) under light illumination (637 nm). **c** Schematic band diagram of the homojunction device with asymmetric Schottky contacts, i.e., E2/WSe_2-S and E3/WSe_2-h, at zero bias

WSe_2-h and WSe_2-S exhibit PC property, and there is no photocurrent at zero bias. In fact, Ti/WSe_2/Ti should be supposed to form a metal/semiconductor/metal structure which contains two Schottky junctions with opposite built-in field. So, the I_d-V_d curves should be cross the zero-point and exhibit PC behavior. In our case, due to the different work functions of WSe_2-h and WSe_2-S, there are two asymmetric Schottky contacts, i.e., E2/WSe_2-S and E3/WSe_2-h, as shown in Fig. 4c. At zero bias, the direction of net photocurrents originated from the Schottky junctions is opposite to that in the homojunction, and the experiment result shown in Fig. 3a is consistent with the latter. Therefore, the homojunction formed between WSe_2-h and WSe_2-S is the reason for the short-circuit photocurrents.

To further demonstrate that the photoresponse at zero bias is attributed to the homojunction, the output properties were investigated through measuring the I_d-V_d curves of the device with the source-drain voltage applied on electrodes E1 and E4. As shown in Figure S3a, the curves, same as the situation in Fig. 3a, also exhibit the PV and PC characteristics. As discussed above, for the former, the photocurrents are attributed to the built-in field of in-plane homojunction formed between WSe_2-S and WSe_2-h. For the latter, the photocurrents are attributed to the collection of photoexcited carriers by the externally applied V_d. The responsivities as a function of the light power for different V_d are summarized in Figure S3b. The responsivities (detectivities) of 0.51 A W^{-1} (2.21 × 10^{12} jones) and 3.55 A W^{-1} (5.54 × 10^{12} jones) are obtained for V_d of 0 V and 1 V, respectively. During the calculation, the effective photosensitive area, i.e., the WSe_2 part between E1 and E4, is 519.4 μm^2. The response time measured at zero bias is shown in Figure S3c and 3d, in which the rising time is 289 μs and the falling time is 281 μs. For the V_d of 1 V (Figure S3e and 3f), the rising and falling time are 278 μs and 250 μs, respectively. The response speed is a little slower than that measured between electrodes E2 and E3, because the relatively long conductive channel increases the photocarrier transmission distance and the probability for the interaction between photocarriers and defects.

Conclusion

In summary, we have demonstrated an in-plane WSe_2 homojunction by electrically tuning partial WSe_2 flake through interface gate. Compared with existing approaches like chemical doping and electrostatic gating by taking advantage of two gate biases, this design gives a more facile rout to realize WSe_2 homojunction. With light illumination, the device produces distinct short-circuit photocurrents with a detectivity of 3.3 × 10^{12} jones. At high bias, the device presents photoconductive characteristic and generates photocurrents with a detectivity of 1.78 × 10^{11} jones. A response time as fast as 106 μs is also obtained simultaneously. Our study provides an efficient and reliable way for the development of high-performance WSe_2-based photodetectors.

Methods

Both WSe_2 and h-BN bulk materials were purchased from Shanghai Onway Technology Co., Ltd. First, the h-BN and WSe_2 flakes were mechanically exfoliated onto a p$^+$-Si/SiO_2 (300 nm) substrate and a poly-dimethyl siloxane (PDMS) layer, respectively. Then, a micromanipulator was used to put the WSe_2 flake, which is adhered to PDMS, onto the target h-BN flake through the microscope to locate the position. Part of WSe_2 flake overlaps the h-BN flake. Finally, the WSe_2 flake was released from PDMS through heating the substrate. The electrodes (Ti/Au) were prepared by electron-beam lithography, metallization, and the lift-off process. Photoresponse measurements were conducted using Agilent B1500

semiconductor parameter analyzer and laser diode with the wavelength of 637 nm.

Supplementary information

Supplementary information accompanies this paper at https://doi.org/10.1186/s11671-020-03342-9.

Additional file 1: Figure S1. Temporal response of the device acquired at V_d = 1 V for 637 nm illumination. **Figure S2.** Photoresponse of the other three devices under 637 nm illumination. **Figure S3** Photoresponse performance of the homojunction acquired between E1 and E4.

Abbreviations

TMDCs: Transition metal dichalcogenides; PV: Photovoltaic; PC: Photoconductive; AFM: Atomic force microscope; IG: Interface gate; PDMS: Poly-dimethyl siloxane

Acknowledgements

This work was supported by the National Natural Science Foundation of China (grant no. 61904203).

Authors' Contributions

NG and LX contributed to the idea of the project. JWC and NG designed and carried out the experiments. YS and LX participated in the analyses of the results and discussion of this work. GHL helped to draft and revise the manuscript. The authors read and approved the final manuscript.

Availability of Data and Materials

The data that support the findings of this work are available from the corresponding author upon reasonable request.

Competing Interests

The authors declare that they have no competing interests.

Author details

[1]Qian Xuesen Laboratory of Space Technology, China Academy of Space Technology, Beijing 100094, China. [2]Department of Materials Science and Engineering, School of Mechanical Electronic & Information Engineering, China University of Mining & Technology, Beijing 100083, China.

Received: 10 March 2020 Accepted: 6 May 2020
Published online: 14 May 2020

References

1. Koppens FHL, Mueller T, Avouris P, Ferrari AC, Vitiello MS, Polini M (2014) Photodetectors based on graphene, other two-dimensional materials and hybrid systems. Nat Nanotechnol 9:780–793
2. Xia F, Wang H, Xiao D, Dubey M, Ramasubramaniam A (2014) Two-dimensional material nanophotonics. Nature Photon 8:899–907
3. Huo N, Konstantatos G (2018) Recent progress and future prospects of 2D-based photodetectors. Adv Mater 27:1801164
4. Fang H, Hu W (2017) Photogating in low dimensional photodetectors. Adv Sci 4:1700323
5. Wang QH, Kalantar-Zadeh K, Kis A, Coleman JN, Strano MS (2012) Electronics and optoelectronics of two-dimensional transition metal dichalcogenides. Nat Nanotechnol 7:699–712
6. Huang Y, Sutter E, Shi NN, Zheng J, Yang T, Englund D, Guo H, Sutter P (2015) Reliable exfoliation of large-area high-quality flakes of graphene and other two-dimensional materials. ACS Nano 9:10612–10620
7. Massicotte M, Schmidt P, Vialla F, Schädler KG, Reserbat-Plantey A, Watanabe K, Taniguchi T, Tielrooij KJ, Koppens FHL (2016) Picosecond photoresponse in van der Waals heterostructures. Nat Nanotechnol 11:42–46
8. Jo SH, Kang DH, Shim J, Jeon J, Jeon M-H, Yoo G, Kim J, Lee J, Yeom GY, Lee S, Yu HY, Choi C, Park JH (2016) A high-performance WSe_2/h-BN photodetector using a triphenylphosphine (PPh3)-based n-doping technique. Adv Mater 28:4824–4831
9. Lopez-Sanchez O, Lembke D, Kayci M, Radenovic A, Kis A (2013) Ultrasensitive photodetectors based on monolayer MoS_2. Nat Nanotechnol 8:497–501
10. Wang X, Wang P, Wang J, Hu W, Zhou X, Guo N, Huang H, Sun S, Shen H, Lin T, Tang M, Liao L, Jiang A, Sun J, Meng X, Chen X, Lu W, Chu J (2015) Ultrasensitive and broadband MoS_2 photodetector driven by ferroelectrics. Adv Mater 27:6575–6581
11. Kang DH, Kim MS, Shim J, Jeon J, Park HY, Jung WS, Yu HY, Pang CH, Lee S, Park JH (2015) High-performance transition metal dichalcogenide photodetectors enhanced by self-assembled monolayer doping. Adv Funct Mater 25:4219–4227
12. Choi MS, Qu D, Lee D, Liu X, Watanabe K, Taniguchi T, Yoo WJ (2014) Lateral MoS_2 p-n junction formed by chemical doping for use in high-performance optoelectronics. ACS Nano 8:9332–9340
13. Hu C, Dong D, Yang X, Qiao K, Yang D, Deng H, Yuan S, Khan J, Lan Y, Song H, Tang J (2017) Synergistic effect of hybrid PbS quantum dots/2D-WSe_2 toward high performance and broadband phototransistors. Adv Funct Mater 27:1603605
14. Huo N, Gupta S, Konstantatos G (2017) MoS_2-HgTe quantum dot hybrid photodetectors beyond 2 μm. Adv Mater 29:1606576
15. Kufer D, Nikitskiy I, Lasanta T, Navickaite G, Koppens FHL, Konstantatos G (2015) Hybrid 2D–0D MoS_2-PbS quantum dot photodetectors. Adv Mater 27:176–180
16. Ma C, Shi Y, Hu W, Chiu MH, Liu Z, Bera A, Li F, Wang H, Li LJ, Wu T (2016) Heterostructured $WS_2/CH_3NH_3PbI_3$ photoconductors with suppressed dark current and enhanced photodetectivity. Adv Mater 28:3683–3689
17. Yu WJ, Liu Y, Zhou H, Yin A, Li Z, Huang Y, Duan X (2013) Highly efficient gate-tunable photocurrent generation in vertical heterostructures of layered materials. Nat Nanotechnol 8:952–958
18. Zhang W, Chiu MH, Chen CH, Chen W, Li LJ, Wee ATS (2014) Role of metal contacts in high-performance phototransistors based on WSe_2 monolayers. ACS Nano 8:8653–8661
19. Yang T, Zheng B, Wang Z, Xu T, Pan C, Zou J, Zhang X, Qi Z, Liu H, Feng Y, Hu W, Miao F, Sun L, Duan X, Pan A (2017) Van der Waals epitaxial growth and optoelectronics of large-scale WSe_2/SnS_2 vertical bilayer p–n junctions. Nat Comm 8:1906
20. Buscema M, Island JO, Groenendijk DJ, Blanter SI, Steele GA, van der Zant HSJ, Castellanos-Gomez A (2015) Photocurrent generation with two-dimensional van der Waals semiconductors. Chem Soc Rev 28:3691–3718
21. Furchi MM, Pospischil A, Libisch F, Burgdörfer J, Mueller T (2014) Photovoltaic effect in an electrically tunable van der Waals heterojunction. Nano Lett 14:4785–4791
22. Long M, Liu E, Wang P, Gao A, Xia H, Luo W, Wang B, Zeng J, Fu Y, Xu K, Zhou W, Lv Y, Yao S, Lu M, Chen Y, Ni Z, You Y, Zhang X, Qin S, Shi Y, Hu W, Xing D, Miao F (2016) Broadband photovoltaic detectors based on an atomically thin heterostructure. Nano Lett 16:2254–2259
23. Das S, Appenzeller J (2013) WSe_2 field effect transistors with enhanced ambipolar characteristics. Appl Phys Lett 103:103501
24. Groenendijk DJ, Buscema M, Steele GA, Michaelis de Vasconcellos S, Bratschitsch R, van der Zant HSJ, Castellanos-Gomez A (2014) Photovoltaic and photothermoelectric effect in a double-gated WSe_2 device. Nano Lett 14:5846–5852
25. Pospischil A, Furchi MM, Mueller T (2014) Solar-energy conversion and light emission in an atomic monolayer p–n diode. Nat Nanotechnol 9:257–261
26. Tang Y, Wang Z, Wang P, Wu F, Wang Y, Chen Y, Wang H, Peng M, Shan C, Zhu Z, Qin S, Hu W (2019) WSe_2 Photovoltaic device based on intramolecular p-n junction. Small 15:1805545
27. Sun J, Wang Y, Guo S, Wan B, Dong L, Gu Y, Song C, Pan C, Zhang Q, Gu L, Pan F, Zhang J (2019) Lateral 2D WSe_2 p-n homojunction formed by efficient charge-carrier-type modulation for high-performance optoelectronics. Adv Mater 32:1906499
28. Baugher BWH, Churchill HOH, Yang Y, Jarillo-Herrero P (2014) Optoelectronic devices based on electrically tunable p–n diodes in a monolayer dichalcogenide. Nat Nanotechnol 9:262–267
29. Cheng R, Li D, Zhou H, Wang C, Yin A, Jiang S, Liu Y, Chen Y, Huang Y, Duan X (2014) Electroluminescence and photocurrent generation from atomically sharp WSe_2/MoS_2 heterojunction p–n diodes. Nano Lett 14:5590–5597
30. Liu C, Yan X, Song X, Ding S, Zhang DW, Zhou P (2018) A semifloating gate memory based on van der Waals heterostructures for quasi-non-volatile applications. Nat Nanotechnol 13:404–410

31. Wu E, Xie Y, Zhang J, Zhang H, Hu X, Liu J, Zhou C, Zhang D (2019) Dynamically controllable polarity modulation of $MoTe_2$ field-effect transistors through ultraviolet light and electrostatic activation. Sci Adv 5: eaav3430
32. Lin YC, Chang CYS, Ghosh RK, Li J, Zhu H, Addou R, Diaconescu B, Ohta T, Peng X, Lu N, Kim MJ, Robinson JT, Wallace RM, Mayer TS, Datta S, Li LJ, Robinson JA (2014) Atomically thin heterostructures based on single-layer tungsten diselenide and graphene. Nano Lett 14:6936–6941
33. Yu X, Prévot MS, Guijarro N, Sivula K (2015) Self-assembled 2D WSe_2 thin films for photoelectrochemical hydrogen production. Nat Commun 6:7596
34. Stenger I, Schué L, Boukhicha M, Berini B, Plaçais B, Loiseau A, Barjon J (2017) Low frequency Raman spectroscopy of few-atomic-layer thick hBN crystals. 2D Mater 4:031003
35. Wang H, Wu Y, Cong C, Shang J, Yu T (2010) Hysteresis of electronic transport in graphene transistors. ACS Nano 4:7221–7228
36. Jeon PJ, Min SW, Kim JS, Raza SRA, Choi K, Lee HS, Lee YT, Hwang DK, Choi HJ, Im S (2015) Enhanced device performances of WSe_2-MoS_2 van der Waals junction p-n diode by fluoropolymer encapsulation. J Mater Chem C 3: 2751–2758
37. Kim K, Larentis S, Fallahazad B, Lee K, Xue J, Dillen DC, Corbet CM, Tutuc E (2015) Band alignment in WSe_2-graphene heterostructures. ACS Nano 9: 4527–4532
38. Huo N, Yang J, Huang L, Wei Z, Li SS, Wei SH, Li J (2015) Tunable polarity behavior and self-driven photoswitching in p-WSe_2/n-WS_2 heterojunctions. Small 11:5430–5438
39. Konstantatos G, Sargent EH (2010) Nanostructured materials for photon detection. Nat Nanotechnol 5:391–400
40. Guo Y, Yu G, Liu Y (2010) Functional organic field-effect transistors. Adv Mater 22:4427–4447
41. Liu X, Gu L, Zhang Q, Wu J, Long Y, Fan Z (2014) All-printable band-edge modulated ZnO nanowire photodetectors with ultra-high detectivity. Nat Comm 5:4007
42. Gong X, Tong M, Xia Y, Cai W, Moon JS, Cao Y, Yu G, Shieh CL, Nilsson B, Heeger AJ (2009) High-detectivity polymer photodetectors with spectral response from 300 nm to 1450 nm. Science 325:1665–1667

Publisher's Note